Zitierweise: *Angew. Chem. Int. Ed.* **2024**, *63*, e202403756
doi.org/10.1002/anie.202403756

Drug Delivery

Light-induced Delivery of Charged Species using Ion-selective Core–Shell Nanoparticles

*Víctor de la Asunción-Nadal, Gastón A. Crespo, and María Cuartero**

Abstract: Controlled release systems have gained considerable attention owing to their potential to deliver molecules, including ions and drugs, in a customized manner. We present a light-induced ion-transfer platform consisting of a dispersion of nanoparticles (NPs, ~300 nm) with the conductive polymer poly(3-octylthiophene-2,5-diyl) (POT) in the core and a potassium (K^+)-selective membrane in the shell. Owing to the photoactive nature of POT, POT NPs can be used for a dual purpose: as a host for positively charged species and as an actuator to trigger the subsequent release. POT^0 and doped POT^+ coexist in the core, allowing K^+ encapsulation in the shell. As POT^0 is photo-oxidized to POT^+, K^+ is released to the (aqueous) dispersion phase to preserve the neutrality of the NPs. This process is reversible and can be simultaneously assessed using the native fluorescence of POT^0 and via potentiometric measurements. The NP structure and its mechanism of action were thoroughly studied with a series of control experiments and complementary techniques. Understanding the NP and its surrounding interactions will pave the way for other nanostructured systems, facilitating sophisticated applications. The delivery of ionic drugs and interference/pollutant catching for advanced sensing/restoration will be considered in future research.

Introduction

Nanoparticle (NP)-based drug delivery systems have received considerable attention because of their potential to improve the efficiency and safety of traditional non-targeted therapies. These systems are engineered to encapsulate a therapeutic drug in nanosized substrates and release it in a controlled manner via a physicochemical trigger, such as light irradiation,[1] magnetic fields,[2] or a chemical gradient.[3] One important feature of this technology is the increased bioavailability of the administered drug compared to traditional methods.[4] Indeed, controlled release systems can focus the administration of therapeutics to a targeted tissue, organ, or cell type, customizing the clinical treatment while avoiding side effects for healthy tissues/organs. By locally targeting the affected body region and selectively releasing the required drug, the dose and frequency of treatment can be minimized while maximizing the positive effects. Furthermore, cross-reactivity and physicochemical degradation may be diminished as a direct consequence of NP encapsulation.[5] Once the clinical target is achieved, and depending on their size and composition, NPs are cleared by the immune system after a certain time, typically ranging from minutes to hours. Interestingly, any interaction with the host immune system can be minimized by modifying the NP surface with proteins, such as albumin.[6,7] Thus, tailoring the NP structure and dimensions makes it feasible to adapt the retention time in the body so that the therapeutic effect is maximized, and any side effects are minimized.

Several materials have been proposed to design NPs intended for drug delivery applications.[8] Indeed, it is possible to provide NPs with adequate biocompatibility and/or enhanced stability,[9] tracking ability through fluorescence imaging,[10] and/or further therapeutic properties (e.g., self-heating or generation of reactive oxygen species).[11] Semiconductor materials, such as transition metal dichalcogenides, have been proposed for simultaneous photodynamic and photothermal therapy.[12] Lipid NPs have been demonstrated as carriers of vaccines,[13] and conductive polymers have been engineered to deliver insulin and diclofenac.[14,15] Specifically, conductive polymers are considered biologically safe, and functional layers can be introduced to increase their biocompatibility or retention time.[16,17] Moreover, owing to their intrinsic semiconducting features, different electrochemical processes can be performed to modify or actuate such materials. For example, once polyaniline (PANI) is electrochemically activated, it releases protons and is an efficient acidification actuator on the microscale[18] with confined local effects.[19] The operation underlying local pH changes generated by activated PANI has been modeled, and, in principle, it could be translated to the NP configuration.[20] Moreover, any conducting polymer's electrochemical, photochemical, or photoelectrochemical behavior is prone to manifest in the NP configuration.[21]

[*] Dr. V. d. la Asunción-Nadal, Prof. G. A. Crespo, Prof. M. Cuartero
Department of Chemistry
KTH, The Royal Institute of Technology
Teknikringen 30, SE-100 44, Stockholm, Sweden
E-mail: mariacb@kth.se
Prof. G. A. Crespo, Prof. M. Cuartero
UCAM-SENS
Universidad Católica San Antonio de Murcia
UCAM HiTech, Avda. Andres Hernandez Ros 1, 30107, Murcia, Spain

Among the available conducting polymers, polythiophenes have gained significant attention in the fields of (bio)sensors, energy generation, and organic electronics. These polymers work based on hole-transport conductivity.[22] Moreover, ion-transfer processes can be analytically exploited when combined with ion-selective membranes in ion-selective electrodes (ISEs) under controlled potential protocols.[23,24] When incorporating a lipophilic cation exchanger, such as sodium tetrakis[3,5-bis(trifluoromethyl)phenyl]borate (Na^+TFPB^-), in the membrane, the conducting polymer backbone can be reversibly doped with $TFPB^-$. This facilitates the generation of positive charges by applying a potential, which ultimately results in a cation transfer at the sample-membrane interface.[25] Moreover, as p-type semiconductor materials, when polythiophenes are irradiated with a suitable wavelength, electron-hole pairs are generated.[26] Combined with the doping process, this can be tuned to achieve selective light-induced doping/dedoping of polythiophene-based NPs. This strategy has already been adopted in the literature, mainly for analytical purposes.[27] The strategy of having poly(3-octylthiophene-2,5-diyl) (POT) in the shell of NPs comprising a cation exchanger and selective receptor for potassium ions (K^+) in the core, has been proposed for use as nanosensors.[28] More studies are needed to clarify the processes involved in the fluorescence modulation in POT-based NPs to exploit their potential in different applications properly, not only as sensors but also for the delivery of charge species that are confined in the NPs.

Herein, we propose a series of NPs with a core–shell POT-membrane structure resembling the traditional architecture of ISEs based on a POT-membrane double-layer configuration.[24] We hypothesized that a series of charge reallocation events may occur by shifting the ratio between neutral (i.e., the base state of POT, POT^0) and oxidized POT (POT^+). This may encapsulate/release ions (in this case, K^+, as a proof of concept) on demand. To demonstrate this, photo-oxidation was imposed on a series of NPs whose shells (i.e., the ion-selective membrane) had different compositions. The NP was strategically loaded with different ionophores and cation exchangers to understand each component's role and synergies upon irradiation. The elucidation of the working mechanism aligns with the encapsulation/delivery features, and thus, applicability beyond traditional ion sensing is proposed. The developed NP technology is promising in terms of providing nanocarriers of charged species, which is useful for the delivery of ionic drugs and interference/pollutant removal.

Results and Discussion

Synthesis and characterization of POT NPs. Figure 1a depicts the process developed for synthesizing the POT-membrane core–shell NPs. Pristine POT NPs were prepared by adding 500 µL of a solution of POT dissolved in THF (50 mg of regioregular POT in 5 mL of THF) to 5 mL of polyvinylalcohol (PVA) solution in water (1 % in mass). The addition was performed dropwise under stirring at 600 rpm in an open vial. With this procedure NPs with a POT-PVA core–shell structure are obtained. Then, to include the ion-selective membrane elements in the NPs shell (plasticizer, cation-exchanger, ionophore), we added dropwise 200 µL of a solution containing 8 mg of valinomycin (K^+ ionophore, Val), 1 mg of Na^+TFPB^- (or another cation exchanger containing a general lipophilic anion R^-, Val : R^- in a

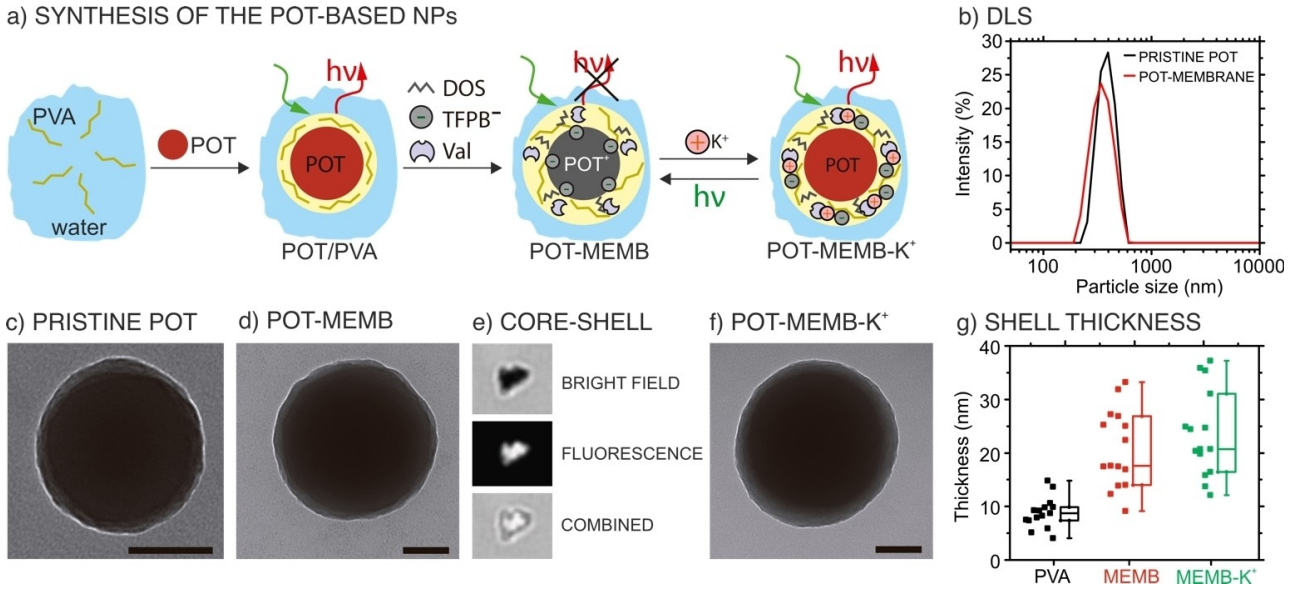

Figure 1. (a) Schematic of the synthesis of the NPs and their fluorescence behavior. (b) DLS size distribution of the pristine POT and POT-membrane NPs. (c) TEM image of a pristine POT NP (POT/PVA). (d) TEM image of a POT-membrane NP (POT/PVA/DOS/Val/R^-). (e) Bright field, fluorescence, and combined bright field and fluorescence microscopy images of the POT-membrane NP. Excitation wavelength: 550 nm. (f) TEM image of the POT-membrane NP incubated in 10 mM KCl for 24 h. (g) Boxplot of the thicknesses measured by TEM of the shell of the different NPs. Scale bars: 100 nm.

6.5:1 mol ratio) and 15 mg of DOS in 1 mL of THF to 1 mL of the pristine POT NP emulsion while stirring for 30 min at 600 rpm in an open vial. To ensure the evaporation of THF, we blew a stream of compressed air on the surface of the dispersion while stirring for 30 min. A 1 mg/mL POT-membrane core–shell NP solution was obtained.

The size of the POT NPs is mainly dictated by the concentration of the stabilizing agent (PVA) and the agitation set by the magnetic stirrer for the preparation process. Regarding the latter, a rotation of 600 rpm was found as the optimal to obtain stable nano-emulsions of a certain NP size (ca. 300 nm, see below). If other NP dimension is desired, an ultrasound-assisted procedure is recommended instead of the mechanical stirring herein used. Smaller NPs will result in shorter times for K^+ uptake accompanied by lower saturation levels and *vice versa.* While interesting, this study is outside the scope of the current work.

Dynamic light scattering (DLS) measurements of the pristine POT and POT-membrane NPs were performed. The data were fit to a lognormal distribution to obtain the mean hydrodynamic particle size (Figure 1b). The pristine POT NPs had an average size of 398 nm with a polydispersity index (PDI) of 0.33, whereas the POT-membrane NPs showed an average size of 368 nm with a PDI of 0.25. Although the hydrodynamic size of NPs largely depends on aggregation occurring during the corresponding measurement, both NPs had similar size distributions using DLS and transmission electron microscopy images (TEM, see below), with only a ca. 25 % difference, which was expected upon comparing these techniques.[29] The obtained PDI implies that POT-based NPs have a rather homogeneous size distribution, which is acceptable for drug delivery applications.[30]

Figures 1c and 1d present TEM images of a single pristine POT NP and a single POT-membrane NP. A clear core–shell structure was revealed, with a shell size of 5–30 nm, where the higher values corresponded to the POT-membrane NPs. The shell is composed of hydrophilic PVA, and thus, it is in contact with the aqueous dispersion, whereas the core is hydrophobic POT. When the PVA contained membrane-like components (plasticizer, exchanger, and ionophore), the shell swelled slightly (~10 nm). This structure was further confirmed with separate bright field and fluorescence microscopy images and their combination (Figure 1e). A higher fluorescence intensity was observed in the core with respect to the shell, corresponding to the fluorescence emission of neutral POT (POT^0) and the absence of significant fluorescence by the shell. The outer layer physically separates the membrane-related components, providing the selective ion-transfer capabilities (i.e., the exchanger and ionophore) and the POT core in the POT-membrane NPs. Notably, to our knowledge, this is the first time that such a core–shell POT-membrane structure has been reported for NPs, and it resembles the architecture of voltammetric ion-selective electrodes in the macro format previously reported by our group for ion analysis.[31,32]

Additionally, we studied the morphology of the POT-membrane NPs when incubated in 10 mM KCl solution for 24 h (the sample was dried overnight upon placing it on a glass slide for imaging). As shown in Figure 1f, no significant swelling or shrinkage of the shell and/or core was observed after incubation. Magnification of the core–shell interfaces of pristine POT and POT-membrane NPs (the latter without and with K^+ incubation) are provided in Figure S1 in the *Supporting Information* for better visualization and comparison. Figure 1g shows the box plot of the measured thickness of the shell presented in the pristine POT and POT-membrane NPs without and with KCl incubation. The thickness of the shell in pristine POT NPs was 9 ± 3 nm. For the POT-membrane NPs, it was 21 ± 7 nm, and for the POT-membrane NPs incubated in 10 mM KCl for 24 h, the thickness was 24 ± 8 nm. A Tukey's range test was performed to assess the differences in the means for the thicknesses of the shells ($\alpha = 0.01$, $n = 15$). The pristine POT showed statistically significant differences from the POT-membrane NPs, whereas incubation did not generate a significant difference.

The zeta potential of POT-membrane NPs in 100 mM Tris buffer was found to be -1.2 ± 0.3 mV, whereas POT-membrane NPs in 100 mM Tris buffer and 10 mM K^+ showed a slightly more negative zeta potential of -2.1 ± 0.4 mV. The decrease in the absolute zeta potential maybe related to the absorption of K^+ into the NPs' structure when the membrane-like shell is presented.

Behavior of POT-based NPs for ion encapsulation. Figure 2a presents the absorbance spectra of solutions containing pristine POT NPs and the POT-membrane NPs in Tris buffer (0.1 M, pH = 7.8) and after 24 h of incubation in 1 M KCl. A Fluoromax Plus fluorometer (Horiba) coupled to a Micromax 384 well-plate reader (Horiba) was used for these experiments, using a sample volume of 150 µL. The pristine POT NP solution *(black line)* exhibited strong fluorescence with two bands from 600 to 800 nm upon irradiation at 550 nm. In contrast, the fluorescence drastically decreased in the POT-membrane NP solution (*red line*). Interestingly, the fluorescence signal recovered almost the same intensity as for the pristine POT NPs when the POT-membrane NPs were incubated in KCl (*green line*). Moreover, this trend was confirmed in the UV-vis absorbance spectra (Figure S2, *Supporting Information*). Because the fluorescent nature of POT is related to its neutral state (POT^0),[33] the experiments suggested that POT^0 is present in the pristine POT NPs, while POT^+ appears in the presence of R^- (which can dope POT^+ in the core) in the membrane. In NPs with a lipophilic anion, POT^0 is mainly present after incubation in KCl because K^+ enters the membrane with the assistance of the ionophore. Therefore, R^- returns to the shell, and POT^+ reverts to POT^0. This mechanism is based on electroneutrality conditions, both in the shell and core phases, and is illustrated in Figure 1a.

The proposed mechanism implies that POT^0, which is known to be the energetically preferred basal state of POT,[34] can be converted to POT^+ upon irradiation at 550 nm and in the presence of R^- in the shell, which can compensate the generated positive charge in POT. Notably, this process will be accompanied by expelling Na^+ (cation part of the cation exchanger) from the NP to the solution.

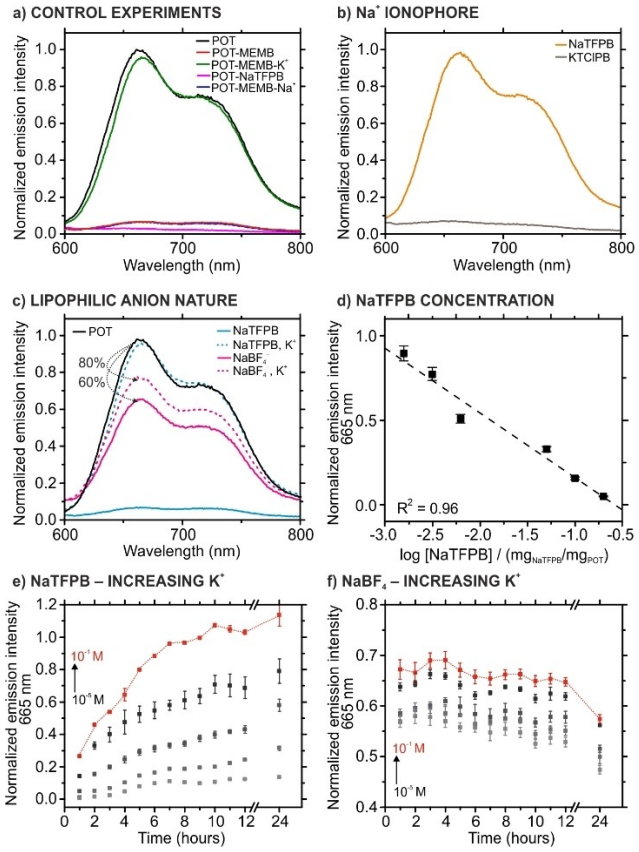

Figure 2. (a) Fluorescence spectra of pristine POT NPs, POT-membrane NPs prepared with the K^+ ionophore and NaTFPB in the absence and presence of incubation in 1 M KCl and 1 M NaCl (66 mM after mixing with the NP solution), and POT-membrane NPs without an ionophore. (b) Fluorescence spectra of NPs containing the Na^+ ionophore and NaTFPB or KTClPB as the cation exchanger. (c) Fluorescence spectra of NPs prepared with NaTFPB or $NaBF_4$ as the cation exchanger (with the K^+ ionophore) in the absence and presence of incubation in 1 M KCl (66 mM after mixing with the NP solution). The spectrum of pristine POT NPs is included for reference. (d) Plot of the logarithmic concentration of NaTFPB in the shell (no ionophore) versus the fluorescence signal at 665 nm upon 550-nm irradiation. (e) Dynamic fluorescence signal at 665 nm under 550 nm irradiation was observed with POT-membrane NPs containing NaTFPB as the cation exchanger, with the NPs being incubated at increasing KCl concentrations. (f) Dynamic fluorescence signal at 665 nm under 550-nm irradiation of POT-membrane NPs containing $NaBF_4$ as the cation exchanger, with the NPs incubated at increasing KCl concentrations. Figures (e) and (f) were normalized to the emission intensity of pristine POT at each time. Notably, each experiment was performed in triplicate (i.e., sample aliquots were placed in three consecutive wells of the plate), finding a variation coefficient $<5\,\%$ in the intensity displayed at 655 nm. While only one spectrum at each condition is shown in panels (a)-(c), error bars are related to the triplicates in panels (d)–(f).

Thus, NPs without containing the K^+ ionophore must display no fluorescence, as the core will be POT^+ doped with R^-. This is what we found in the related experiments (*pink line*, Figure 2a). Moreover, other authors reported on the formation of POT^+ (and other polythiophenes derivatives) was possible upon irradiation (visible at 510 nm or UV at 420 nm) in the presence of O_2. For example, poly(3-hexylthiophene) (PHT) can be photoinduced to a singlet excited state PHT*(S_1) that evolves to PHT^+/O_2^- ion pairs, which can thus result in chemical interactions of PHT^+-O_2^-.[35,36] This behavior could translate into POT^+/R^- charge pair formation in our NPs only when R^- is available.

Of note, R^- is unavailable to doped POT^+ when the POT-membrane NPs are incubated with K^+, because R^- is the counter anion of the ionophore-K^+ complex formed in the membrane-like shell. The formation of such a complex is energetically favored ($\log\beta_{K^+-\text{valinomycin}} = 9.3$ in the membrane phase).[37] Thus, the single NP reaches an energetic state based on the ionophore of K^+/R^-, which is more favorable than that with the POT^+/R^- pair. Indeed, when the POT-membrane NPs were incubated in 1 M NaCl, with Na^+ less preferred than K^+ by the ionophore ($\log\beta_{Na^+-\text{valinomycin}} = 6.4$ in the membrane phase),[37] no fluorescence was observed (*blue line*, Figure 2a), in contrast to the situation when KCl incubation was accomplished.

To be more precise, the only case showing a flat fluorescence spectrum was the NP solution without the K^+ ionophore, i.e., the NP does not have any preference to capture cations from the solution. The other NPs displayed two pronounced bands, indicating a POT^0/POT^+ ratio in the core of differing degrees. This depends on the R^- availability in the PVA phase. Overall, the competition between POT^+ and ionophore-M^+ (M^+ = any cation) by R^- in the NPs results in selective encapsulation of the cation upon irradiation.

The selectivity of the POT-membrane NPs for K^+ is dictated by the ionophore, i.e., valinomycin, in analogy to ion-selective membranes of similar compositions. It is known that the main interference in valinomycin-based systems selective for K^+ will be Na^+ (logarithmic selectivity coefficient calculated for membranes of $\log K_{K,Na} = -4.2$).[38] Also, Na^+ will be the main possibly interfering ion considering biological samples. In our experiments, POT-membrane NPs incubated in high concentration (up to 1 M) of Na^+ for long times (up to 24 hours) showed negligible Na^+ uptake, displaying similar fluorescence recovery as the blank solution (Figure 2a). This result pointed out the high selectivity of the NPs toward K^+ uptake versus Na^+.

Replacing the K^+ ionophore with the Na^+ ionophore revealed similar trends, confirming the proposed ion encapsulation mechanism, and demonstrating the versatility of the NP platform to selectively encapsulate different cations. This also showed the importance of the appropriate selection of the cation exchanger, which must not contain the cation of interest if customized encapsulation is desired. As observed in Figure 2b, when the cation in the exchanger salt was Na^+, POT^+ did not form, as evidenced by the high fluorescence of the corresponding curve (*orange line*, Figure 2b) due to the presence of POT^0 in the core. This is because the ionophore-Na^+ complex originally formed in the NP upon its synthesis and the complex attracts most of the R^-. Hence, POT^0 cannot be converted to POT^+. In contrast, potassium tetrakis(4-chlorophenyl)borate (K^+ $TClPB^-$) allowed Na^+ encapsulation, as deduced from the absence of fluorescence (*grey line*, Figure 2b) related to the

presence of POT^+ in the core. Given these results, it is possible to directly encapsulate a target cation in the NP during its synthesis, when the cation is available as a cation exchanger and the corresponding selective ionophore is considered. In any case, the cation can be encapsulated after incubation of the NPs prepared with a cation exchanger not containing such a cation and the corresponding ionophore, which is a universal approach for encapsulation.

Influence of the nature and concentration of the lipophilic anion in the encapsulation mechanism. The nature of the lipophilic anion in the cation exchanger and its concentration may influence the mechanism and the corresponding fluorescence signal, in terms of magnitude and kinetics, of the NPs. To study this, we synthesized a POT-membrane NP emulsion with sodium tetrafluoroborate ($Na^+BF_4^-$) as the cation exchanger instead of Na^+TFPB^-, maintaining the same molar concentration. Notably, BF_4^- is smaller and less lipophilic than $TFPB^-$. The fluorescence spectra of NPs based on Na^+TFPB^- or $Na^+BF_4^-$ in the absence and presence of incubation in a 1 M KCl solution are presented in Figure 2c. Two main aspects are shown. First, the fluorescence was lower when we used $TFPB^-$ *(blue solid line*, Figure 2c*)* than when BF_4^- was used (*pink dotted line*, Figure 2c). Compared with the original fluorescence displayed by the pristine POT NPs *(black line*, Figure 2c*)*, the decreases in fluorescence were approximately 100 and 60 %, respectively. Second, the fluorescence recovery after incubation in KCl was also different, with recoveries of 100 % *(blue dashed line)* and 80 % *(pink dashed line)* of the original fluorescence of the pristine POT NPs for $TFPB^-$ and BF_4^-, respectively.

The effect of the concentration of the lipophilic anion on the fluorescence signal was evaluated by decreasing the NaTFPB concentration in the NPs (original content: 0.2 mg_{NaTFPB}/mg_{POT}) and obtaining the emission spectra (Figure S3, *Supporting Information*). The experiment was performed using NPs without the K^+ ionophore. However, similar results were expected when the ionophore was utilized because no incubation steps were performed (i.e., no K^+ in the system). The fluorescence was found to increase with decreasing NaTFPB concentration. Moreover, at a fluorescence emission of 665 nm, the plot of the normalized intensity (considering the signal of pristine POT NPs as 1.0) with the logarithm of NaTFPB concentration is shown in Figure 2d, revealing a linear relationship ($R^2 = 0.96$). This behavior is explained by the fact that less NaTFPB in the membrane results in less POT^+ formed. Thus, the fluorescence is expected to continuously increase until it resembles the fluorescence of pristine POT NPs. Why is this trend linear with a logarithmic NaTFPB concentration instead of a direct concentration? For different NaTFPB concentrations, different Na^+ concentrations are likely expelled from each NP into the solution. This results in a different potential at the sample-membrane interface. Such a potential is known to follow the Nernst equation (i.e., linear with the logarithmic concentration of Na^+ in the sample) in POT-membrane systems analogous to the NP structure in this study.[23,31] Because the POT/POT^+ ratio in the core providing the fluorescence intensity depends on available R^- in the membrane, which connects to the expelled Na^+ generating the membrane potential, the intensity may ultimately depend on the logarithmic R^- concentration.

Concerning the kinetics, we performed dynamic studies of the fluorescence signal in POT-membrane NPs prepared with NaTFPB or $NaBF_4$ upon incubation in 0.1 M KCl (final concentration of K^+ in the solution of 66 mM after mixing with the NPs). Figures 2e and 2f show the fluorescence at 665 nm under 550 nm irradiation for the two different NPs *(red lines)*. In principle, a higher incubation time could be expected to result in more K^+ encapsulated in the membrane. Thus, a higher fluorescence signal (closer to that of pristine POT NPs) results. According to the literature, the uptake of K^+ may occur on the timescale of seconds,[39] and hence, any time-dependent fluorescence increase will be related to particular changes in the molecular structure of the POT core.[40] In our experiments, the rearrangement of the POT structure in the NP core seems to occur on the timescale of hours in the case of NaTFPB, with a gradual increase of the fluorescence until the 10 h. After that, a steady-state fluorescence signal was achieved. In contrast, a constant signal was recorded for the NPs based on $NaBF_4$, with no considerable fluorescence increase detected with time. The same fluorescence behavior was found for decreasing KCl concentrations in the incubation solution (Figure 2e and Figure 2f). The trends found for $TFPB^-$ and BF_4^- indeed agree with previous findings because small ions, such as BF_4^-, are known to have a small influence on the crystallinity of poly(3-alkylthiophenes), which will facilitate the generation of the fluorescence signal.[41]

To our understanding, a change in the lipophilic anion has two effects: i) different oxidation degrees of the POT core, i.e., from POT^0 to POT^+, decreasing the original fluorescence of pristine POT NPs, and ii) different effect on the crystalline domains in the POT structure, which are responsible for an enhanced fluorescence signal by the restriction of intramolecular motion (RIM). An increase in the mobile amorphous fraction with non-radiative energy dissipation paths has been shown to occur.[42,43] The smaller size of BF_4^- with respect to $TFPB^-$ will have less effect on the supramolecular structure of the POT backbone in the core. Then, because BF_4^- is less hydrophobic than $TFPB^-$, the tendency to reach the POT core will be lower. The balance of all these factors is key to understanding the lower fluorescence decrease (c.a. 100 % compared to ~60 %) observed when BF_4^- is used as a cation exchanger instead of $TFPB^-$. Overall, the hydrophobic feature of the $TFPB^-$ ensures a quantifiable fluorescence decay due to the appropriate formation of POT^+ in the NP core, which indicates that more K^+ can be introduced into the NP structure via encapsulation. This allows us to tailor the NP synthesis with different K^+ loading capacities, depending on the concentration of NaTFPB in the shell, which will be relevant to future loading/release Schemes for real applications.

Concentration-dependent photo-induced ion encapsulation into POT-based NPs. Subsequently, we evaluated the effect of the KCl concentration in the incubation solution on

the K^+ amount encapsulated in the membrane. The concentration range was from 10^{-5} to 10^{-1} M, with 0.1 M Tris buffer (pH = 7.8) as the background. These solutions were mixed in a 2:1 (KCl:NPs) ratio with NPs prepared with NaTFPB or $NaBF_4$ as the cation exchanger. The initial fluorescence spectrum was obtained at t = 0, when the corresponding NP solution was added to the KCl solution. Then, the spectrum was recorded every hour until 12 h and then after 24 h. The signal at 665 nm was selected to create the dynamic profiles presented in Figures 2e and 2f for NaTFPB NPs and $NaBF_4$ NPs, respectively.

In both cases, increasing K^+ concentrations in the solution resulted in a higher fluorescence, and this effect was more prominent in the case of NaTFPB. Thus, K^+ encapsulation in the shell was demonstrated to occur: some of the POT^+ in the core becomes POT^0, with released R^- overseeing the pairing of the K^+ ionophore complex, therefore maintaining the overall neutrality of the NP. At increasing K^+ concentrations, the fluorescence tends to approach that displayed by the pristine POT NPs. This behavior is much clearer in the case of NaTFPB. As discussed above, when the nature of the lipophilic anion was evaluated, a higher amount of K^+ is encapsulated with longer incubation times, which resulted in a higher fluorescence signal until a steady state was reached. This occurred at ca. 10 h for NaTFPB and at 1 h for $NaBF_4$ at all the assayed concentrations, which was expected according to the mobility of each anion.

Figure 3a presents the plots of the fluorescence signals at 665 nm (24 h of incubation for $TFPB^-$ and 12 h for BF_4^-, according to the previous results) with the logarithmic concentration of K^+ in the samples of NaTFPB NPs and $NaBF_4$ NPs. Acceptable linearity was found in both cases, and the sensitivity for the NaTFPB NPs was higher than that for $NaBF_4$ NPs (0.248 vs. 0.026). Interestingly, along with the wide dynamic range given by the logarithmic dependence of the fluorescence with the K^+ concentration, the higher sensitivity of NPs loaded with NaTFPB makes them a valuable alternative for nanosensing applications, as previously reported in the literature for other NP systems.[28]

Ion-release behavior of POT-based NPs. The fluorescence of POT-membrane NPs (with NaTFPB) incubated for 24 h in solutions of increasing K^+ concentrations were assessed upon continuous irradiation with a 550-nm LED lamp using an inverted microscope fluorescence setup. We measured 2 μL of each sample containing a 1:2 volume ratio of NPs and K^+ solution, ensuring complete exposure to the light source. Upon irradiation, the fluorescence decreased until reaching a steady-state signal at approximately 60 s (Figure 3c). In contrast, for the sample containing NPs in buffer and no K^+, the fluorescence was constant over the entire experiment *(purple line)*. We hypothesized that after spontaneous K^+ encapsulation in the NPs (during the 24-h incubation process), K^+ is released back to the sample upon LED irradiation, as indicated by the fluorescence decrease. This phenomenon was not observed in the fluorescence experiments with the fluorometer because of the higher light density (3.5 W cm^{-2}) and lower sample volume used.

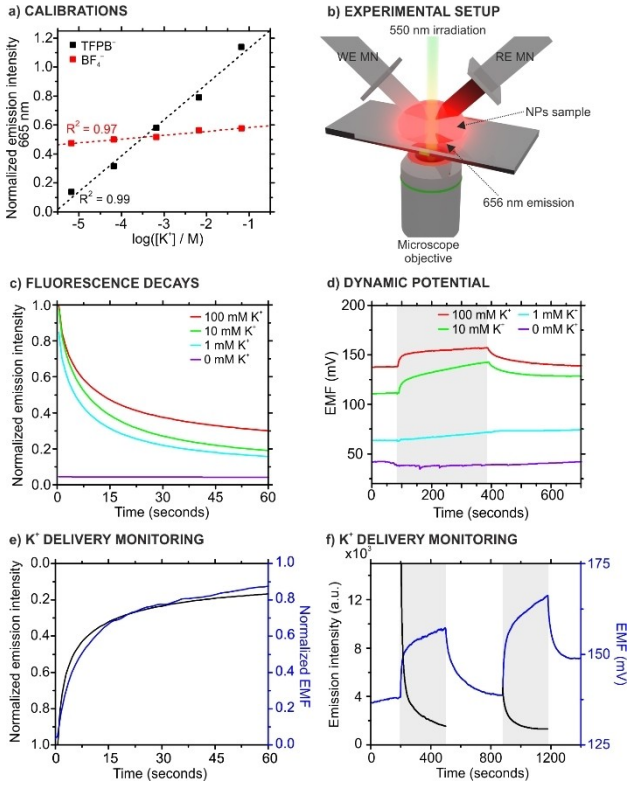

Figure 3. (a) Normalized emission intensity of the POT-membrane NPs using NaTFPB (black line) and $NaBF_4$ (red line) as the cation exchanger with different concentrations of K^+. (b) Experimental setup used to perform the fluorescence microscopy experiments. The K^+ concentration in the sample was monitored using potentiometric microneedles. WE MN: working electrode microneedle. RE MN: reference electrode microneedle. (c) Real-time microscale fluorescence measurements of POT-membrane NPs incubated in different concentrations of K^+ for 24 h before irradiation. (d) Dynamic K^+ concentration profiles obtained using the microneedles before, during, and after irradiation at 550 nm (gray background = irradiation ON). (e) Normalized fluorescence intensity (black line) and normalized electromotive force (EMF) of the POT-membrane NPs incubated in a solution containing 100 mM K^+ for 24 h under 550-nm irradiation. (f) In situ monitoring of the K^+ delivery processes according to the fluorescence intensity (black) and EMF (blue) under 550-nm irradiation (gray background = irradiation ON).

To confirm that the light-induced fluorescence decrease was unequivocally due to K^+ delivery from the NPs, we monitored the K^+ concentration in the sample using a potentiometric microneedle-based sensor. The (K^+-selective) indicator and reference electrodes were prepared as reported elsewhere.[44] Figure 3b and Figure S4 show how the microneedles were positioned in the microscopy setup. Notably, these were positioned not to interrupt the light path (see Figure S5). The microneedle format was used to miniaturize the potentiometric setup so that it can be used with the reduced sample volume utilized in the microscope, which is needed to trigger the release of K^+ and record the emission from the NPs simultaneously. The potentiometric signal of the solution was recorded before, during, and after irradiation at 550 nm. The profiles are shown in Figure 3d. Upon irradiation, the K^+ concentration rapidly increased in

the solution until it reached a steady state in approximately 1 min, as revealed by the increase in the potential (electromotive force, EMF). This behavior confirmed the K^+ release from the NPs into the solution. A gradual return to a lower K^+ concentration was observed when the light was off. We detected the achievement of the initial K^+ concentration in the solution only in the case of the 100-mM incubation solution.

Upon semi-quantitative analysis, we observed percent increases of 14, 36, and 11 % from the initial K^+ concentration when the steady-state potential was reached during irradiation of the 1-, 10- and 100-mM samples (the K^+ concentrations were fixed in the standard solutions used for mixing with the NPs). Furthermore, the K^+ uptake was confirmed with a control experiment using pristine POT NPs incubated with the 100-mM KCl solution. A constant dynamic potential was observed before, during, and after irradiation (Figure S6), confirming the absence of any K^+ release or uptake. Interestingly, for the case of the POT-membrane NPs incubated with the 100-mM KCl solution, when the fluorescence signal of the NPs and the potential measured in the solution were normalized (from 0 to 1) and compared, the profiles revealed similar behavior (Figure 3e). This highlighted two findings: i) what occurs in the NPs reflects in the solution and *vice versa* and ii) both results (fluorescence and potentiometry) follow a similar dependence with K^+ concentration in solution (i.e., a logarithmic dependence).

Interestingly, when the irradiation applied to the NP sample after incubation in 100 mM KCl was intermittent (two ON-OFF cycles of 300 s each), a slight fluorescence recovery was observed between the irradiation pulses (Figure 3f, *black line*). This recovery was attributed to the re-incorporation of K^+ from the medium to the NP shell. The experiments revealed that the delivery/uptake process can be repeated up to five consecutive times (Figure S7), demonstrating the reversibility of the cation uptake/release process. Notably, a higher number of cycles was not possible to be assessed because the effect of the evaporation of the sample. Moreover, monitoring the K^+ concentration in the medium using the microneedle sensor confirmed the increase and decrease of K^+ within the ON-OFF cycles (Figure 3f, *blue line*). These results are additional experimental evidence of the spontaneous K^+ uptake by the NPs and the light-driven K^+ delivery to the sample.

The emission decay was recorded at varying power densities and considering different KCl concentrations in the sample solution (1000 mM, 100 mM, 10 mM and 1 mM). A power-law decay was observed, with an $I_{em}(a.u.) = a(a.u.)\ (1 + t(ms))^b$ trend (Figure S8a). Interestingly, the *a* and *b* parameters showed a correlation with the irradiation intensity (Figure S8b) but not with the concentration. This result evidenced the dependence of the cation delivery process with the irradiation intensity.

To assess the effect of the ionic strength of the samples on the K^+ uptake/delivery process, experiments with different Tris concentrations (100 mM, 10 mM, and 1 mM) were performed. The POT-membrane NPs were incubated for 24 h in the buffer solutions additionally containing 100 mM K^+ and the typical fluorescence decay experiment was accomplished (Figure S9). The curves overlapped between them, indicating that the uptake and delivery of K^+ were not affected by the ionic strength of the solution. Moreover, to discard possible matrix interferences when using the NPs in real samples in a near future, experiments in horse serum were performed. An aliquot of POT-membrane NPs was incubated for 24 h in horse serum, in which the K^+ concentration was assessed by ion chromatography ($[K^+] = 2.41$ mM). In parallel, another aliquot was incubated in a buffer solution with the same concentration of K^+. The delivery and reuptake of K^+ were recorded for both solutions, displaying no significant differences in the results (Figure S10), also considering kinetics.

Proposed mechanism of ion encapsulation and delivery using POT-membrane NPs. As a summary of all the information from the previous experimental evidence, Figure 4a provides a visual representation of the mechanism involved in the encapsulation and release of K^+ in POT NPs, linked this with a modulation in the original fluorescence form pristine POT NPs. In addition, the reader is kindly referred to the *Supporting Information (Section 1.8)* for a summary of the reactions taking place when the NP-sample interface is considered. First, the pristine (POT-PVA core–shell) NPs were modified with membrane-like components: a plasticizer, cation exchanger, and ionophore. The oxidation of the POT core is enhanced upon introducing a lipophilic anion in the shell that can stabilize the generated positive charge. Two processes were found to experimentally occur simultaneously: i) slight swelling of the PVA shell, which could be related to the introduction of the plasticizer, and ii) a decrease in the fluorescence of the

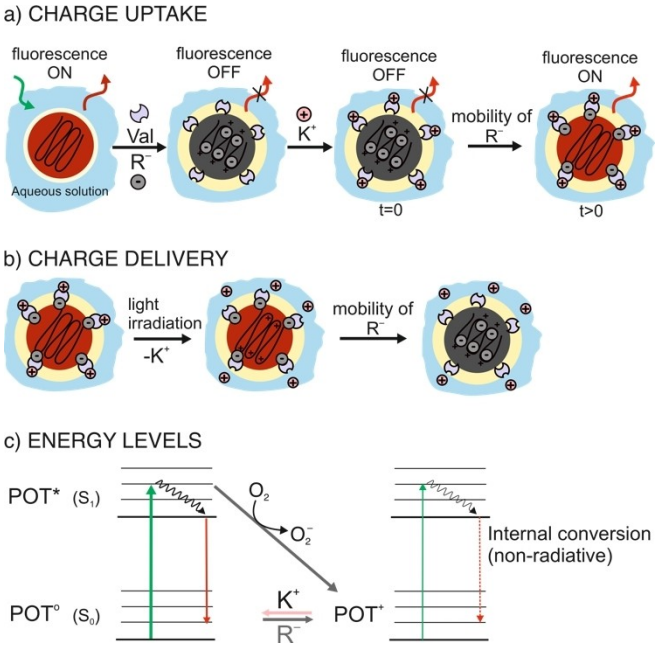

Figure 4. (a) Ionophore-assisted cation uptake to the NPs. (b) Light-induced cation release from the NPs. (c) Diagram of the main steps involved in the fluorescence process.

pristine POT NPs. The latter confirmed the oxidation of the POT and the stabilization of the formed POT^+ by the lipophilic anion (R^-), which followed the RIM effect. When valinomycin-based NPs are incubated with K^+, this cation penetrates the NP shell and forms a charged K^+-valinomycin complex paired with (R^-). This implies undoping of the POT core, breaking the POT^+-R^- interaction, and leading to the recovery of the native POT fluorescence. Light-driven K^+ delivery, when encapsulated in the NP shell, was possible (Figure 4b), and this could be monitored by fluorescence and potentiometry measurements. POT is a photoactive material that can be oxidized under light and oxygen with sufficient irradiation density. In the case of NPs, the POT core can be partially converted to POT^+ through photooxidative processes, as previously reported for other POT configurations/structures.[36]

Figure 4c illustrates a Jablonski diagram with the proposed mechanism according to the literature and our experimental evidence herein obtained.[39] Thus, pristine POT^0 is in the fluorescent state when synthesized, and the non-fluorescent state (POT^+) can be obtained by chemically doping the polymer with a lipophilic anion (R^-) or by photooxidation in the presence of molecular oxygen. The presence of oxygen is required for this process to happen. Indeed, according to electron paramagnetic resonance studies applied to the photooxidation process of poly(3-hexylthiophene) (P) in presence and absence of molecular oxygen, the formation of P^+/O^{2-} was demonstrated as an intermediate metastable state. It is herein assumed that POT will behave similarly as this polymer (same family).[36] To confirm this, POT NPs were modified with NaTFPB in nitrogen-saturated solutions. The fluorescence signal was found to be significantly higher in the absence of oxygen (Figure S11a), meaning that oxygen acts as an electron acceptor in the POT doping process. Moreover, the signal was found to decrease with time due to the gradual presence of oxygen in the NPs solution (Figure S11b).

When the polymer core is in the non-fluorescent (POT^+) state, the fluorescence can be achieved by incorporating cations with the assistance of the ionophore, forming POT^0. By irradiating the NPs, the equilibrium can be displaced toward forming the non-fluorescent POT^+ state, releasing the cations inside the NPs' structure. In the NPs, generating positive charges in the POT core forces K^+ delivery from the shell to the sample to maintain the electroneutrality. The packing/structure of the polymer chains is affected, considering that R^- enters the lattice to dope the generated positive charge, decreasing the fluorescence. Finally, it is possible to correlate this decrease in fluorescence with the K^+ delivery from the NP into the solution via potentiometry, demonstrating the controlled light-enabled delivery of charged species.

Conclusion

The ion-transfer capabilities (i.e., encapsulation and release) of core–shell POT-based NPs were demonstrated in this study. Comprising a membrane-like shell loaded with different ion exchangers and ionophores, the NPs have different fluorescence levels depending on the POT/POT^+ ratio in the core. Accordingly, the fluorescence changes provided an understanding of the ability of the POT-membrane NPs to incorporate cations into their structures selectively. The overall process involves the ability of the NP to introduce lipophilic anions (part of the ion exchanger) from the shell into the core and *vice versa* and thus doping/undoping the POT/POT^+ core, an encapsulating/releasing in turn the desired cation (e.g., K^+ or Na^+). The working mechanism is highly dependent on the nature of the lipophilic anion: $TFPB^-$ presented better cation uptake abilities than BF_4^-. Moreover, the fluorescence signal had a linear relationship with the logarithmic concentration of the cation in the sample solution. While cation encapsulation occurs via direct incubation of the NPs in the corresponding sample, cation delivery from the NP (after its encapsulation) is a light-driven process requiring a specific irradiation wavelength. Thus, the photooxidation of POT to POT^+ in the core was used for controlled cation delivery from the NP to the solution, which was monitored via fluorescence and potentiometry measurements. On-off cycles of irradiation allowed for subsequent delivery/encapsulation of K^+ (as proof of concept) from/to the NPs, which is a time-dependent process. Future efforts should focus on the on-demand encapsulation/delivery of clinically relevant charged species (e.g., amino acids, drugs) and/or the development of advanced sensing systems on the nanoscale.

Acknowledgements

This project received funding from the European Research Council (ERC) under the European Union's Horizon 2020 Research and Innovation Programme (grant agreement no. 851957). M.C. and V.A.N. acknowledge the Carl Tryggers Foundation (20:88). The authors thank Agueda Molinero-Fernandez for helping with the microneedle measurements.

Conflict of Interest

The authors declare no conflict of interest.

Data Availability Statement

The data that support the findings of this study are available from the corresponding author upon reasonable request.

Keywords: nanoparticles · conductive polymers · ion-selective membranes · ion encapsulation · light-induced ion delivery

[1] C. Alvarez-Lorenzo, L. Bromberg, A. Concheiro, *Photochem. Photobiol.* **2009**, *85*, 848–860.
[2] E. Kianfar, *J. Supercond. Novel Magn.* **2021**, *34*, 1709–1735.
[3] M. Karzar Jeddi, M. Mahkam, *Int. J. Biol. Macromol.* **2019**, *135*, 829–838.

[4] M. Vallet-Regí, F. Schüth, D. Lozano, M. Colilla, M. Manzano, *Chem. Soc. Rev.* **2022**, *51*, 5365–5451.
[5] A. K. Rashwan, N. Karim, Y. Xu, J. Xie, H. Cui, M. R. Mozafari, W. Chen, *Crit. Rev. Food Sci. Nutr.* **2021**, DOI 10.1080/10408398.2021.1987858.
[6] S. Lamichhane, S. Lee, *Arch. Pharmacal Res.* **2020**, *43*, 118–133.
[7] N. Hosseinifar, A. A. M. Sharif, N. Goodarzi, M. Amini, R. Dinarvand, *J Nanostructure Chem* **2017**, *7*, 327–335.
[8] A. Jayakumar, S. Mathew, S. Radoor, J. T. Kim, J. W. Rhim, S. Siengchin, *Mater. Today Chem.* **2023**, *30*, DOI: 10.1016/j.mtchem.2023.101492.
[9] A. N. Frickenstein, S. Mukherjee, T. Harcourt, Y. He, V. Sheth, L. Wang, Z. Malik, S. Wilhelm, *Anal. Bioanal. Chem.* **2023**, DOI 10.1007/s00216-023-04540-*x*.
[10] Z. Liu, B. Yun, Y. Han, Z. Jiang, H. Zhu, F. Ren, Z. Li, *Adv. Healthcare Mater.* **2022**, *11*, DOI: 10.1002/adhm.202102042.
[11] V. de la Asunción-Nadal, C. Franco, A. Veciana, S. Ning, A. Terzopoulou, S. Sevim, X. Z. Chen, D. Gong, J. Cai, P. D. Wendel-Garcia, B. Jurado-Sánchez, A. Escarpa, J. Puigmartí-Luis, S. Pané, *Small* **2022**, *18*, DOI: 10.1002/smll.202203821.
[12] J. Yu, W. Yin, X. Zheng, G. Tian, X. Zhang, T. Bao, X. Dong, Z. Wang, Z. Gu, X. Ma, Y. Zhao, *Theranostics* **2015**, *5*, 931–945.
[13] R. Tenchov, R. Bird, A. E. Curtze, Q. Zhou, *ACS Nano* **2021**, *15*, 16982–17015.
[14] C. Chen, X. Chen, H. Zhang, Q. Zhang, L. Wang, C. Li, B. Dai, J. Yang, J. Liu, D. Sun, *Acta Biomater.* **2017**, *55*, 434–442.
[15] N. Hosseini-Nassab, D. Samanta, Y. Abdolazimi, J. P. Annes, R. N. Zare, *Nanoscale* **2017**, *9*, 143–149.
[16] A. S. Widge, M. Jeffries-El, X. Cui, C. F. Lagenaur, Y. Matsuoka, *Biosens. Bioelectron.* **2007**, *22*, 1723–1732.
[17] J. W. Shreffler, J. E. Pullan, K. M. Dailey, S. Mallik, A. E. Brooks, *Int. J. Mol. Sci.* **2019**, *20*, DOI: 10.3390/ijms20236056.
[18] F. Steininger, A. Wiorek, G. A. Crespo, K. Koren, M. Cuartero, *Anal. Chem.* **2022**, *94*, 13647–13651.
[19] C. Chen, A. Wiorek, A. Gomis-Berenguer, G. A. Crespo, M. Cuartero, *Anal. Chem.* **2023**, *95*, 4180–4189.
[20] A. F. Molina-Osorio, A. Wiorek, G. Hussain, M. Cuartero, G. A. Crespo, *J. Electroanal. Chem.* **2021**, *903*, DOI: 10.1016/j.jelechem.2021.115851.
[21] K. Kłucińska, E. Jaworska, K. Maksymiuk, A. Michalska, *Electroanalysis* **2017**, *29*, 2167–2176.
[22] B. S. Ong, Y. Wu, P. Liu, S. Gardner, *J. Am. Chem. Soc.* **2004**, *126*, 3378–3379.
[23] Y. Liu, G. A. Crespo, M. Cuartero, *Anal. Chem.* **2022**, *94*, 9140–9148.
[24] M. Cuartero, G. A. Crespo, E. Bakker, *Anal. Chem.* **2016**, *88*, 1654–1660.
[25] E. M. Therézio, J. L. Duarte, E. Laureto, E. Di Mauro, I. L. Dias, A. Marletta, H. De Santana, *J. Phys. Org. Chem.* **2011**, *24*, 640–645.
[26] N. Banerji, S. Cowan, E. Vauthey, A. J. Heeger, *J. Phys. Chem. C* **2011**, *115*, 9726–9739.
[27] A. Kisiel, E. Woźnica, K. Maksymiuk, A. Michalska, *Sens. Actuators B* **2017**, *238*, 160–165.
[28] K. Kłucińska, E. Stelmach, A. Kisiel, K. Maksymiuk, A. Michalska, *Anal. Chem.* **2016**, *88*, 5644–5648.
[29] T. G. F. Souza, V. S. T. Ciminelli, N. D. S. Mohallem, in *J Phys Conf Ser*, Institute Of Physics Publishing, **2016**.
[30] M. Danaei, M. Dehghankhold, S. Ataei, F. Hasanzadeh Davarani, R. Javanmard, A. Dokhani, S. Khorasani, M. R. Mozafari, *Pharmaceutica* **2018**, *10*, DOI: 10.3390/pharmaceutics10020057.
[31] Y. Liu, G. A. Crespo, M. Cuartero, *Electrochim. Acta* **2021**, *388*, DOI: 10.1016/j.electacta.2021.138634.
[32] K. Xu, Y. Liu, G. A. Crespo, M. Cuartero, *Electrochim. Acta* **2022**, *427*, DOI: 10.1016/j.electacta.2022.140870.
[33] T. Danno, K. Kobayashi, A. Tanioka, *J. Appl. Polym. Sci.* **2006**, *100*, 3111–3115.
[34] J. P. Veder, R. De Marco, K. Patel, P. Si, E. Grygolowicz-Pawlak, M. James, M. T. Alam, M. Sohail, J. Lee, E. Pretsch, E. Bakker, *Anal. Chem.* **2013**, *85*, 10495–10502.
[35] Y. Aoyama, T. Yamanari, T. N. Murakami, T. Nagamori, K. Marumoto, H. Tachikawa, J. Mizukado, H. Suda, Y. Yoshida, *Polym. J.* **2015**, *47*, 26–30.
[36] A. Aguirre, S. C. J. Meskers, R. A. J. Janssen, H. J. Egelhaaf, *Org. Electron.* **2011**, *12*, 1657–1662.
[37] E. Bakker, M. Wilier, M. Lerchl, K. Seller, *Anal. Chem.* **1994**, *66*, 516–521.
[38] R. Cánovas, S. Padrell Sánchez, M. Parrilla, M. Cuartero, G. A. Crespo, *ACS Sens.* **2019**, *4*, 2524–2535.
[39] X. Xie, J. Zhai, G. A. Crespo, E. Bakker, *Anal. Chem.* **2014**, *86*, 8770–8775.
[40] Y. Aoyama, O. Douhéret, P. Leclère, D. Moerman, J. Mizukado, H. Suda, R. Lazzaroni, Y. Yoshida, *Org. Electron.* **2017**, *43*, 142–147.
[41] K. N. Baustert, A. Abtahi, A. N. Ayyash, K. R. Graham, *J. Polym. Sci.* **2022**, *60*, 602–609.
[42] Y. Tu, Z. Zhao, J. W. Y. Lam, B. Zhong Tang, *Natl. Sci. Rev.* **2021**, *8*.
[43] Y. Aoyama, O. Douhéret, P. Leclère, D. Moerman, J. Mizukado, H. Suda, R. Lazzaroni, Y. Yoshida, *Org. Electron.* **2017**, *43*, 142–147.
[44] Á. Molinero-Fernández, A. Casanova, Q. Wang, M. Cuartero, G. A. Crespo, *ACS Sens.* **2023**, *8*, 158–166.

Manuscript received: February 22, 2024
Accepted manuscript online: March 19, 2024
Version of record online: March 28, 2024